Robotica (2013) volume 31, pp. 511–523. © Cambridge University Press 2012
doi:10.1017/S0263574712000525

Dynamic grasping of an arbitrary polyhedral object

Akihiro Kawamura*, Kenji Tahara, Ryo Kurazume and Tsutomu Hasegawa

Graduate School of Information Science and Electrical Engineering, Kyushu University, Fukuoka, 819-0395, Japan

(Accepted July 25, 2012. First published online: October 1, 2012)

SUMMARY

This paper proposes a novel dynamic stable grasping method of an arbitrary polyhedral object for a hand-arm system with hemispherical fingertips. This method makes it possible to satisfy the force/torque equilibrium condition for the immobilization of the object without knowledge of the object. Two control signals are proposed which generate grasping forces normal and tangential to an object surface in a final state. The dynamics of the overall system is modeled and analyzed theoretically. We demonstrate the stable grasping of an arbitrary polyhedral object using the proposed controller through numerical simulations and experiments using a newly developed mechanical hand-arm system.

KEYWORDS: Grasping; Redundant Manipulators; Robot Dynamics; Robotic Hands; Control of Robotic Systems.

1. Introduction

Grasping and manipulation of an object is the most fundamental and necessary function for robots that operate around our living space. Until now, several robotic systems and their control methods intended to accomplish stable object grasping have been proposed.[1–5] In particular, the multi-fingered robotic hand system is one of the most expected devices for an end-effector because it is capable of human-like dexterous manipulation. Most existing methods for the multi-fingered robotic hand system consider static or quasi-static situations, and the form/force closure concept is used to evaluate grasping quality.[6] In these methods, precise information on the grasped object, such as its geometric shape, mass, and the position of the center of mass, is necessary for stable grasping and manipulation. Furthermore, the contact position of each fingertip and the position and attitude of the object are required in real-time. A great deal of computation time is also required for planning a manipulation task.

In contrast, dynamic stable object grasping methods proposed by Arimoto *et al.*[7–9] for a pair of robotic fingers use neither object nor contact information. Their controller is based on the fingers-thumb opposability concept, and a dynamic force/torque equilibrium condition is realized using the rolling motion of spherical fingertips,[10–13] even though the form/force closure condition is not satisfied. In their method, each hemispherical fingertip rolls along the object surface so as to converge the overall movement. As a result, the dynamic force/torque equilibrium condition is satisfied when the overall system is in the steady state. Tahara *et al.*[14,15] later extended Arimoto's method to a three-fingered robotic hand system. However, they treated only a cuboid as a grasped object. Moreover, their method requires the dynamic force/torque equilibrium condition to be satisfied using only the individual normal force components on the contact surface. This requirement is too strict and difficult to be satisfied, even for a cuboid. Therefore, they introduced a compensation term to relax this requirement. This term is given as the time integral of each joint angular velocity and quite effective for attaining the force/torque equilibrium condition more easily than in the case of using only the individual normal force components. However, the force derived from the integral term in the final state cannot be estimated theoretically in advance because the force increases according to the total movement of each joint angle. This leads to another problem that the integral term disturbs the manipulation of the grasped object.

This paper proposes a novel method of object grasping for a multi-fingered hand-arm system. An artificial relative attitude constraint is introduced between each finger, instead of integrating the angular velocity of each joint with respect to time. This artificial constraint is the most significant difference compared to the studies by Arimoto and Tahara.[7–9,14,15] The constraint does not require any object information similar to the integral term proposed by Tahara.[14,15] A constraint force based on the artificial relative attitude constraint plays almost the same role as the time integration of each joint angular velocity. However, the force does not disturb any other control signals, such as that for stable grasping and manipulation, because the artificial constraint restricts only the relative attitude between each fingertip by a P-feedback and is independent of other control signals if the system has a sufficient number of degrees of freedom (DOFs). In addition, since the artificial constraint purely works to enhance the region of stable grasping, our method achieves dynamic stable grasping of an arbitrary polyhedral-shaped object without any external sensing devices. In other words, the method does not require any object information, such as the shape, mass, or position of the center of mass of the object, even though

* Corresponding author. E-mail: kawamura@irvs.ait.kyushu-u.ac.jp

the shape of a graspable object is extended to an arbitrary polyhedron.

Furthermore, we propose a coordinate controller for a robotic arm part in addition to a multi-fingered hand part unlike the studies of Arimoto *et al.* and Tahara *et al.*[7–9, 14, 15] The robotic arm system is indispensable for a hand system to approach and manipulate an object in a practical situation. Therefore, we design a unified controller to simultaneously control both a multi-fingered hand part and an arm part. Bae *et al.*[16] proposed a unified controller to grasp and manipulate an object using the hand-arm system. However, their controller considered only a two-dimensional (2-D) model, and the grasped object has been assumed to be a rectangular parallelepiped. We improve Bae *et al.*'s[16] method so as to be applicable for grasping an arbitrary polyhedral object in 3-D space.

In the following, we first formulate a nonholonomic rolling constraint between each hemispherical fingertip and the surface of a grasped object. Arimoto *et al.*[7–9, 14, 15] modeled one of the rolling constraints, which can be easily expressed in an equation of motion. However, the object has been assumed to have two flat and parallel surfaces. Therefore, we extend their rolling constraint model so as to express the constraint for an arbitrary polyhedral object. Then we derive the overall equation of motion that considers the effect of the rolling constraint. Next, a control signal to satisfy dynamic stable grasping of an arbitrary polyhedral object is designed, and the stability of the overall system is verified based on the passivity theory. Through numerical simulations and experiments using a prototype multi-fingered robotic hand system, we demonstrate the stable grasping of an arbitrary polyhedral object using the proposed controller.

The advantages of the proposed method in comparison with the previous methods proposed by Arimoto *et al.* or Tahara *et al.*[7–9, 14, 15] are listed as follows:

(1) The proposed method achieves stable grasping of an arbitrary polyhedral object. The graspable object shape is expanded.
(2) A new control signal $\boldsymbol{u}_{st}$ is proposed. It acts purely to restrict unnecessary rolling motion of each fingertip.
(3) The facts (1) and (2) are verified by analyzing a closed-loop dynamics of the overall system. These are shown in equilibrium manifold of the overall system.
(4) The proposed method does not disturb and interfere with manipulation motion in combination with a position and attitude controller for the grasped object. The position and attitude of the grasped object converges to the desired position and attitude precisely.
(5) We reformulate and expand the rolling constraints model proposed by Arimoto *et al.*[7–9, 14, 15] so as to express the constraint for an arbitrary polyhedral object.
(6) We design a unified controller to simultaneously control both the multi-fingered hand part and the arm part.

In this paper, we extend our previous work[17] and show the following new contents:

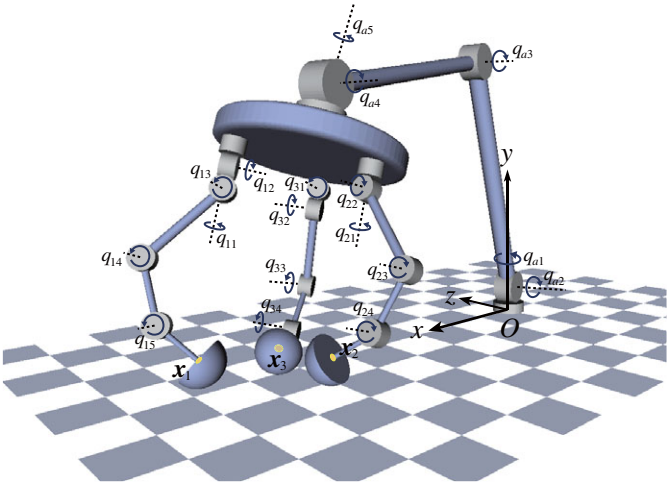

Fig. 1. (Colour online) Multi-fingered hand-arm system.

(1) An elicitation process of each mathematical formula is added in more detail.
(2) A theoretical stability analysis of the overall system is conducted and discussed more deeply.
(3) A practical usefulness of the proposed method is demonstrated through some experiments using a prototype of the three-fingered robotic hand system.

2. Overall Model

In this section, the overall model, which is composed of a multi-fingered hand-arm system and a grasped object, is presented. The hand-arm system is composed of a serial-link arm part and a multi-fingered hand part. In the modeling, a nonholonomic rolling constraint between each fingertip and the object surface is modeled in order to consider physical interaction between the multi-fingered hand-arm system and the grasped object. The rolling constraint modeled here is based on Arimoto *et al.*'s model[7, 8, 14, 15] and is enhanced so as to be applicable to an arbitrary polyhedral-shaped object. An example of the multi-fingered hand-arm system treated herein is illustrated in Fig. 1. Each finger has soft and hemispherical tips. The assumptions of the present study are listed as follows:

(1) The overall system has a sufficient number of DOFs to stably grasp an object.
(2) Each fingertip maintains rolling contact with the object surface and does not slip or detach from the surface during grasping.
(3) Fingertips do not transition from an initially contacted surface to other surfaces during grasping.
(4) Each joint has high backdrivability.
(5) The mass of the grasped object is small enough to ignore the gravity effect.

As shown in Fig. 1, O denotes the origin of the Cartesian coordinate system, and $\boldsymbol{x}_i \in \mathbb{R}^3$ is the center of each fingertip. In the following, the subscript i indicates the ith finger in all equations. The number of DOFs of the arm and the ith finger are N_a and N_i respectively. A vector of the joint angle of the arm is $\boldsymbol{q}_a \in \mathbb{R}^{N_a}$, and a vector of the joint angle of each of

https://doi.org/10.1017/S0263574712000525 Published online by Cambridge University Press

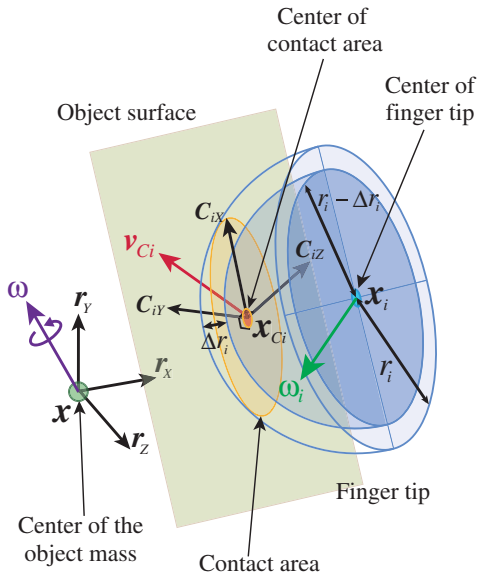

Fig. 2. (Colour online) Contact model at the center of the contact area.

the i fingers is $\boldsymbol{q}_i \in \mathbb{R}^{N_i}$. The symbol $\boldsymbol{q}$ denotes the vector of the joint angle of the entire system, including the arm and all fingers $(= (\boldsymbol{q}_a, \boldsymbol{q}_1, \boldsymbol{q}_2, \ldots, \boldsymbol{q}_N)^{\mathrm{T}})$, where N is the number of fingers. As shown in Fig. 2, $\boldsymbol{x}_{Ci} \in \mathbb{R}^3$ is the center of each contact area. The velocity vector of the center of each contact area is $\boldsymbol{v}_{Ci} \in \mathbb{R}^3$. The radius of each fingertip is r_i. The position of the center of the object mass is $\boldsymbol{x} = (x, y, z)^{\mathrm{T}} \in \mathbb{R}^3$, which also stands for the origin of a local object frame. An instantaneous rotational axis of the object at $\boldsymbol{x}$ expressed in Cartesian coordinates is $\boldsymbol{\omega} = (\omega_x, \omega_y, \omega_z)^{\mathrm{T}} \in \mathbb{R}^3$. In addition, $\boldsymbol{\omega}_i \in \mathbb{R}^3$ signifies the attitude angular velocity vector of the center of each fingertip.

2.1. Constraints

A 3-D rolling constraint with area contact is modeled here. The attitude of the object in Cartesian coordinates can be expressed by a rotational matrix $\boldsymbol{R}$ such that

$$\boldsymbol{R} = \left(\boldsymbol{r}_x, \boldsymbol{r}_y, \boldsymbol{r}_z\right) \in SO(3), \tag{1}$$

where $\boldsymbol{r}_x, \boldsymbol{r}_y, \boldsymbol{r}_z \in \mathbb{R}^3$ are mutually orthonormal vectors that indicate each axis of the local object frame. The rotational matrix is one of the members of $SO(3)$ and satisfies the following equations:

$$\dot{\boldsymbol{R}} = [\boldsymbol{\omega}\times]\,\boldsymbol{R}, \quad [\boldsymbol{\omega}\times] = \begin{pmatrix} 0 & -\omega_z & \omega_y \\ \omega_z & 0 & -\omega_x \\ -\omega_y & \omega_x & 0 \end{pmatrix}. \tag{2}$$

In addition, we define a local contact frame at the center of each contact area in the following:

$$\boldsymbol{R} \cdot \boldsymbol{R}_{Ci} = (\boldsymbol{C}_{iX}, \boldsymbol{C}_{iY}, \boldsymbol{C}_{iZ}), \tag{3}$$

where $\boldsymbol{R}_{Ci}$ is the rotational matrix between the object frame and each contact frame. A unit vector $\boldsymbol{C}_{iY}$ that indicates the y-axis of the contact frame is taken as being normal to the contact surface. When each fingertip is purely rolled along the surface, the velocity vector of the center of each contact area $\boldsymbol{v}_{Ci}$ must satisfy the following relation:

$$\boldsymbol{v}_{Ci} = (r_i - \Delta r_i)\left(\dot{\boldsymbol{C}}_{iY} - \boldsymbol{\omega}_i \times \boldsymbol{C}_{iY}\right), \tag{4}$$

where

$$\Delta r_i = r_i + Y_i - \boldsymbol{C}_{iY}^{\mathrm{T}}(\boldsymbol{x} - \boldsymbol{x}_i). \tag{5}$$

In Eq. (4), Δr_i denotes the displacement due to the deformation of each fingertip at the center of the contact area (see Fig. 2). By definition, the velocity vector $\boldsymbol{v}_{Ci}$ is on the object surface at the center of each contact area. In Eq. (5), Y_i is the perpendicular distance between the center of the object mass $\boldsymbol{x}$ and the surface. The rolling constraint is expressed such that the velocity of the center of each contact area on the fingertip, given as Eq. (4), must be equal to that on the object surface and is given as follows:

$$\begin{bmatrix} \boldsymbol{C}_{iX}^{\mathrm{T}} \\ \boldsymbol{C}_{iZ}^{\mathrm{T}} \end{bmatrix} \boldsymbol{v}_{Ci} = \begin{bmatrix} \dot{X}_i \\ \dot{Z}_i \end{bmatrix}, \tag{6}$$

where

$$X_i = -\boldsymbol{C}_{iX}^{\top}(\boldsymbol{x} - \boldsymbol{x}_i), \tag{7}$$

$$Z_i = -\boldsymbol{C}_{iZ}^{\top}(\boldsymbol{x} - \boldsymbol{x}_i). \tag{8}$$

Equation (6) denotes a nonholonomic rolling constraint between each fingertip and the object surface.

Next, the rolling constraint can be expressed as the Pfaffian constraint as follows:

$$\begin{bmatrix} \boldsymbol{X}_{iq} \\ \boldsymbol{Z}_{iq} \end{bmatrix} \dot{\boldsymbol{q}} + \begin{bmatrix} \boldsymbol{X}_{ix} \\ \boldsymbol{Z}_{ix} \end{bmatrix} \dot{\boldsymbol{x}} + \begin{bmatrix} \boldsymbol{X}_{i\omega} \\ \boldsymbol{Z}_{i\omega} \end{bmatrix} \boldsymbol{\omega} = \boldsymbol{0}, \tag{9}$$

where

$$\begin{bmatrix} \boldsymbol{X}_{iq} = (r_i - \Delta r_i)\,\boldsymbol{C}_{iZ}^{\mathrm{T}}\boldsymbol{J}_{\Omega i} - \boldsymbol{C}_{iX}^{\mathrm{T}}\boldsymbol{J}_i \\ \boldsymbol{X}_{ix} = \boldsymbol{C}_{iX}^{\mathrm{T}} \\ \boldsymbol{X}_{i\omega} = \{\boldsymbol{C}_{iX} \times (\boldsymbol{x} - \boldsymbol{x}_i)\}^{\mathrm{T}} - (r_i - \Delta r_i)\,\boldsymbol{C}_{iZ}^{\mathrm{T}} \\ \boldsymbol{Z}_{iq} = -(r_i - \Delta r_i)\,\boldsymbol{C}_{iX}^{\mathrm{T}}\boldsymbol{J}_{\Omega i} - \boldsymbol{C}_{iZ}^{\mathrm{T}}\boldsymbol{J}_i \\ \boldsymbol{Z}_{ix} = \boldsymbol{C}_{iZ}^{\mathrm{T}} \\ \boldsymbol{Z}_{i\omega} = \{\boldsymbol{C}_{iZ} \times (\boldsymbol{x} - \boldsymbol{x}_i)\}^{\mathrm{T}} + (r_i - \Delta r_i)\,\boldsymbol{C}_{iX}^{\mathrm{T}} \end{bmatrix}. \tag{10}$$

In these equations, $\boldsymbol{J}_i \in \mathbb{R}^{3\times(N_a+\sum_{i=1}^{N} N_i)}$ and $\boldsymbol{J}_{\Omega_i} \in \mathbb{R}^{3\times(N_a+\sum_{i=1}^{N} N_i)}$ denote the Jacobian matrices for the velocity and the angular velocity of the fingertip with respect to the joint angular velocity $\dot{\boldsymbol{q}} \in \mathbb{R}^{N_a+\sum_{i=1}^{N} N_i}$ and are given as follows:

$$\begin{bmatrix} \dot{\boldsymbol{x}}_i \\ \boldsymbol{\omega}_i \end{bmatrix} = \begin{bmatrix} \boldsymbol{J}_i \\ \boldsymbol{J}_{\Omega i} \end{bmatrix} \dot{\boldsymbol{q}}. \tag{11}$$

Using the rolling constraint expressed in Eq. (6), the relationship among $\dot{\boldsymbol{q}}$, $\dot{\boldsymbol{x}}$, and $\boldsymbol{\omega}$ can be given as follows:

$$\begin{bmatrix} \dot{\boldsymbol{x}} \\ \boldsymbol{\omega} \end{bmatrix} = \begin{bmatrix} \boldsymbol{J}_{Cxi} \\ \boldsymbol{J}_{C\omega i} \end{bmatrix} \dot{\boldsymbol{q}}, \tag{12}$$

https://doi.org/10.1017/S0263574712000525 Published online by Cambridge University Press

where

$$\begin{cases} \boldsymbol{J}_{Cxi} = \frac{1}{d_3^2 - d_1 d_2} \left\{ \left(d_2 \boldsymbol{X}_{ix}^{\mathrm{T}} - d_3 \boldsymbol{Z}_{ix}^{\mathrm{T}} \right) \boldsymbol{X}_{iq} \right. \\ \quad \left. + \left(d_1 \boldsymbol{Z}_{ix}^{\mathrm{T}} - d_3 \boldsymbol{X}_{ix}^{\mathrm{T}} \right) \boldsymbol{Z}_{iq} \right\} \\ \boldsymbol{J}_{C\omega i} = \frac{1}{d_3^2 - d_1 d_2} \\ \left\{ \left(d_2 \boldsymbol{X}_{i\omega}^{\mathrm{T}} - d_3 \boldsymbol{Z}_{i\omega}^{\mathrm{T}} \right) \boldsymbol{X}_{iq} + \left(d_1 \boldsymbol{Z}_{i\omega}^{\mathrm{T}} - d_3 \boldsymbol{X}_{i\omega}^{\mathrm{T}} \right) \boldsymbol{Z}_{iq} \right\} \\ d_1 = 1 + \boldsymbol{X}_{i\omega}^2 \\ d_2 = 1 + \boldsymbol{Z}_{i\omega}^2 \\ d_3 = \boldsymbol{X}_{i\omega} \boldsymbol{Z}_{i\omega}^{\mathrm{T}} \end{cases} \tag{13}$$

2.2. Contact model of soft fingertip

In the present paper, a physical relationship between deformation of the soft fingertip at the center of each contact area and its reproducing force is given based on the lumped-parameterized model proposed by Arimoto *et al.*[7] The reproducing force f_i in the normal direction to the object surface at the center of each contact area is given as follows:

$$\begin{cases} f_i = \bar{f}_i + \xi_i \Delta \dot{r}_i \\ \bar{f}_i = k_i \Delta r_i^2 \end{cases}, \tag{14}$$

where k is a positive nonlinear elastic coefficient of the material of the fingertip, and ξ_i is a positive nonlinear damping coefficient function with respect to Δr_i. This indicates that the viscous force depends on the contact area.

In addition, there is another viscosity between each fingertip and the object surface that affects the torsional motion of the fingertip on the object surface. The energy dissipation function based on the torsional viscosity of a fingertip is given as follows:

$$T_i = \frac{b_i}{2} \left|\left| \boldsymbol{C}_{iY}^{\mathrm{T}} \left(\boldsymbol{\omega} - \boldsymbol{\omega}_i \right) \right|\right|^2, \tag{15}$$

where b_i is the coefficient of viscosity, which depends on the fingertip material and the contact area.

2.3. Overall dynamics

The total kinetic energy of the overall system is expressed as follows:

$$K = \frac{1}{2} \dot{\boldsymbol{q}}^{\mathrm{T}} \boldsymbol{H} \dot{\boldsymbol{q}} + \frac{1}{2} \dot{\boldsymbol{x}}^{\mathrm{T}} \boldsymbol{M} \dot{\boldsymbol{x}} + \frac{1}{2} \boldsymbol{\omega}^{\mathrm{T}} \boldsymbol{I} \boldsymbol{\omega}, \tag{16}$$

where $\boldsymbol{H} \in \mathbb{R}^{(N_a + \sum_{i=1}^{N} N_i) \times (N_a + \sum_{i=1}^{N} N_i)}$ is the inertia matrix of the hand-arm system, and $\boldsymbol{M} = \mathrm{diag}\,(m, m, m)$ is the mass of the grasped object. In addition, $\boldsymbol{I} = \boldsymbol{R} \bar{\boldsymbol{I}} \boldsymbol{R}^{\mathrm{T}}$, and $\bar{\boldsymbol{I}} \in \mathbb{R}^{3 \times 3}$, is the inertia tensor of the object represented by the principal axes of inertia.

On the other hand, the total potential energy of the overall system is given as follows:

$$P = P_g \left(\boldsymbol{q} \right) + \sum_{i=1}^{N} P_i, \tag{17}$$

where $P_g \left(\boldsymbol{q} \right)$ is the potential energy for the hand-arm system caused by the effect of gravity, and P_i is the elastic potential energy for the ith finger generated by the deformation of the soft fingertip and expressed as

$$P_i = \int_0^{\Delta r_i} \bar{f}_i \left(\zeta \right) d\zeta. \tag{18}$$

Eventually, Lagrange's equation of motion can be obtained by applying the variational principle in the following form:
For the multi-fingered hand-arm system:

$$\boldsymbol{H} \left(\boldsymbol{q} \right) \ddot{\boldsymbol{q}} + \left\{ \frac{1}{2} \dot{\boldsymbol{H}} \left(\boldsymbol{q} \right) + \boldsymbol{S}_q \left(\boldsymbol{q}, \dot{\boldsymbol{q}} \right) \right\} \dot{\boldsymbol{q}} + \sum_{i=1}^{N} \frac{\partial T_i}{\partial \dot{\boldsymbol{q}}}^{\mathrm{T}} + \sum_{i=1}^{N} \left(\boldsymbol{J}_i^{\mathrm{T}} \boldsymbol{C}_{iY} f_i + \boldsymbol{X}_{iq}^{\mathrm{T}} \lambda_{iX} + \boldsymbol{Z}_{iq}^{\mathrm{T}} \lambda_{iZ} \right) + \boldsymbol{g} \left(\boldsymbol{q} \right) = \boldsymbol{u}. \tag{19}$$

For the grasped object:

$$\boldsymbol{M} \ddot{\boldsymbol{x}} + \sum_{i=1}^{N} \left(-f_i \boldsymbol{C}_{iY} + \boldsymbol{X}_{ix}^{\mathrm{T}} \lambda_{iX} + \boldsymbol{Z}_{ix}^{\mathrm{T}} \lambda_{iZ} \right) = \boldsymbol{0}, \tag{20}$$

$$\boldsymbol{I} \dot{\boldsymbol{\omega}} + \left\{ \frac{1}{2} \dot{\boldsymbol{I}} + \boldsymbol{S}_\omega \right\} \boldsymbol{\omega} - \sum_{i=1}^{N} \{ \boldsymbol{C}_{iY} \times (\boldsymbol{x} - \boldsymbol{x}_i) \} f_i + \sum_{i=1}^{N} \frac{\partial T_i}{\partial \boldsymbol{\omega}}^{\mathrm{T}} + \sum_{i=1}^{N} \left(\boldsymbol{X}_{i\omega}^{\mathrm{T}} \lambda_{iX} + \boldsymbol{Z}_{i\omega}^{\mathrm{T}} \lambda_{iZ} \right) = \boldsymbol{0}, \tag{21}$$

where $\boldsymbol{S}_q$ and $\boldsymbol{S}_\omega$ are the skew-symmetric matrices of the hand-arm system and the grasped object, $\boldsymbol{g}$ is the gravitational terms, and $\boldsymbol{u}$ is the vector of the input torque. In addition, λ_{iX} and λ_{iZ} denote Lagrange's multipliers.

Equations (19)–(21) can now be represented as follows:

$$\boldsymbol{G} \ddot{\boldsymbol{\Lambda}} + \left(\frac{1}{2} \dot{\boldsymbol{G}} + \boldsymbol{S} + \boldsymbol{T} \right) \dot{\boldsymbol{\Lambda}} + \boldsymbol{P}^{\mathrm{T}} \boldsymbol{\lambda} + \boldsymbol{Q}^{\mathrm{T}} \boldsymbol{f} + \boldsymbol{g}_{\mathrm{all}} = \boldsymbol{U}, \tag{22}$$

https://doi.org/10.1017/S0263574712000525 Published online by Cambridge University Press

where

$$\begin{bmatrix} \boldsymbol{G} = \mathrm{diag}\,(\boldsymbol{H}, \boldsymbol{M}, \boldsymbol{I}) \\ \boldsymbol{S} = \mathrm{diag}\left(\boldsymbol{S}_{\mathrm{q}}, \boldsymbol{0}_{3\times3}, \boldsymbol{S}_{\omega}\right) \\ \boldsymbol{T} = \mathrm{diag}\left(\sum_{\mathrm{i}=1}^{\mathrm{N}} \boldsymbol{C}_{\mathrm{T_i}}, \boldsymbol{0}_{3\times3}, 2\boldsymbol{J}_{\mathrm{C}\omega\mathrm{i}} \sum_{\mathrm{i}=1}^{\mathrm{N}} \boldsymbol{C}_{\mathrm{T_i}} \boldsymbol{J}_{\mathrm{C}\omega\mathrm{i}}^{\mathrm{T}}\right) \\ \boldsymbol{C}_{T_i} = b_i \left\{\boldsymbol{C}_{iY}^{\mathrm{T}} \left(\boldsymbol{J}_{C\omega i} - \boldsymbol{J}_{\Omega i}\right)\right\}^{\mathrm{T}} \left\{\boldsymbol{C}_{iY}^{\mathrm{T}} \left(\boldsymbol{J}_{C\omega i} - \boldsymbol{J}_{\Omega i}\right)\right\} \\ \boldsymbol{P} = \begin{bmatrix} \boldsymbol{X}_{1q} & \boldsymbol{X}_{1x} & \boldsymbol{X}_{1\omega} \\ \boldsymbol{X}_{2q} & \boldsymbol{X}_{2x} & \boldsymbol{X}_{2\omega} \\ \vdots & \vdots & \vdots \\ \boldsymbol{X}_{Nq} & \boldsymbol{X}_{Nx} & \boldsymbol{X}_{N\omega} \\ \boldsymbol{Z}_{1q} & \boldsymbol{Z}_{1x} & \boldsymbol{Z}_{1\omega} \\ \boldsymbol{Z}_{2q} & \boldsymbol{Z}_{2x} & \boldsymbol{Z}_{2\omega} \\ \vdots & \vdots & \vdots \\ \boldsymbol{Z}_{Nq} & \boldsymbol{Z}_{Nx} & \boldsymbol{Z}_{N\omega} \end{bmatrix} \\ \boldsymbol{\lambda} = (\lambda_{1X}, \lambda_{2X}, \cdots, \lambda_{NX}, \lambda_{1Z}, \lambda_{2Z}, \cdots, \lambda_{NZ})^{\mathrm{T}} \\ \boldsymbol{Q} = \begin{bmatrix} \boldsymbol{C}_{1Y}^{\mathrm{T}} \boldsymbol{J}_1 & -\boldsymbol{C}_{1Y}^{\mathrm{T}} & (\boldsymbol{x} - \boldsymbol{x}_1)^{\mathrm{T}} [\boldsymbol{C}_{1Y}\times] \\ \boldsymbol{C}_{2Y}^{\mathrm{T}} \boldsymbol{J}_2 & -\boldsymbol{C}_{2Y}^{\mathrm{T}} & (\boldsymbol{x} - \boldsymbol{x}_2)^{\mathrm{T}} [\boldsymbol{C}_{2Y}\times] \\ \vdots & \vdots & \vdots \\ \boldsymbol{C}_{NY}^{\mathrm{T}} \boldsymbol{J}_N & -\boldsymbol{C}_{NY}^{\mathrm{T}} & (\boldsymbol{x} - \boldsymbol{x}_N)^{\mathrm{T}} [\boldsymbol{C}_{NY}\times] \end{bmatrix} \\ \boldsymbol{f} = (f_1, f_2, \cdots, f_N)^{\mathrm{T}} \\ \boldsymbol{g}_{\mathrm{all}} = \left(\boldsymbol{g}^{\mathrm{T}}, \boldsymbol{0}_{1\times6}\right)^{\mathrm{T}} \end{bmatrix}, \tag{23}$$

where $\boldsymbol{U}(=(\boldsymbol{u}^{\mathrm{T}}, \boldsymbol{0}_{1\times6})^{\mathrm{T}})$ denotes an input vector, and $\dot{\boldsymbol{\Lambda}}(=(\dot{\boldsymbol{q}}^{\mathrm{T}}, \dot{\boldsymbol{x}}^{\mathrm{T}}, \boldsymbol{\omega}^{\mathrm{T}})^{\mathrm{T}})$ denotes an output vector of the overall system. From Eq. (23), there exists $\boldsymbol{G}^{-1}$, since $\boldsymbol{G}$ is a positive-definite symmetric matrix. Thereby, the following equation is obtained by pre-multiplying Eq. (22) by $\boldsymbol{P}\boldsymbol{G}^{-1}$:

$$\boldsymbol{P}\ddot{\boldsymbol{\Lambda}} + \boldsymbol{P}\boldsymbol{G}^{-1}\left(\frac{1}{2}\dot{\boldsymbol{G}} + \boldsymbol{S} + \boldsymbol{T}\right)\dot{\boldsymbol{\Lambda}} + \boldsymbol{P}\boldsymbol{G}^{-1}\boldsymbol{P}^{\mathrm{T}}\boldsymbol{\lambda} + \boldsymbol{P}\boldsymbol{G}^{-1}\boldsymbol{Q}^{\mathrm{T}}\boldsymbol{f} + \boldsymbol{P}\boldsymbol{G}^{-1}\boldsymbol{g}_{\mathrm{all}} = \boldsymbol{P}\boldsymbol{G}^{-1}\boldsymbol{U}. \tag{24}$$

Then, from Eq. (9), we obtain

$$\boldsymbol{P}\dot{\boldsymbol{\Lambda}} = 0. \tag{25}$$

By differentiating Eq. (25) with respect to time t, we also obtain

$$\boldsymbol{P}\ddot{\boldsymbol{\Lambda}} = -\dot{\boldsymbol{P}}\dot{\boldsymbol{\Lambda}}. \tag{26}$$

By substituting Eq. (26) into Eq. (24), Eq. (24) is rearranged as follows:

$$\boldsymbol{P}\boldsymbol{G}^{-1}\boldsymbol{P}^{\mathrm{T}}\boldsymbol{\lambda} = \left\{\dot{\boldsymbol{P}} - \boldsymbol{P}\boldsymbol{G}^{-1}\left(\frac{1}{2}\dot{\boldsymbol{G}} + \boldsymbol{S} + \boldsymbol{T}\right)\right\}\dot{\boldsymbol{\Lambda}} - \boldsymbol{P}\boldsymbol{G}^{-1}\boldsymbol{Q}^{\mathrm{T}}\boldsymbol{f} - \boldsymbol{P}\boldsymbol{G}^{-1}\boldsymbol{g}_{\mathrm{all}} + \boldsymbol{P}\boldsymbol{G}^{-1}\boldsymbol{U}. \tag{27}$$

There exists $\left(\boldsymbol{P}\boldsymbol{G}^{-1}\boldsymbol{P}^{\mathrm{T}}\right)^{-1}$ because $\boldsymbol{P}$ is of full rank as long as each rolling constraint is satisfied. Therefore, $\boldsymbol{\lambda}$ can be expressed as follows:

$$\boldsymbol{\lambda} = \left(\boldsymbol{P}\boldsymbol{G}^{-1}\boldsymbol{P}^{\mathrm{T}}\right)^{-1}\left[\left\{\dot{\boldsymbol{P}} - \boldsymbol{P}\boldsymbol{G}^{-1}\left(\frac{1}{2}\dot{\boldsymbol{G}} + \boldsymbol{S} + \boldsymbol{T}\right)\right\}\dot{\boldsymbol{\Lambda}} - \boldsymbol{P}\boldsymbol{G}^{-1}\boldsymbol{Q}^{\mathrm{T}}\boldsymbol{f} - \boldsymbol{P}\boldsymbol{G}^{-1}\boldsymbol{g}_{\mathrm{all}} + \boldsymbol{P}\boldsymbol{G}^{-1}\boldsymbol{U}\right]. \tag{28}$$

Equations (5) and (14) indicate that $\boldsymbol{f}$ can be expressed as a function with respect to $\left(\boldsymbol{\Lambda}, \dot{\boldsymbol{\Lambda}}\right)$. Similarly, $\boldsymbol{\lambda}$ can be expressed as a function with respect to $\left(\boldsymbol{\Lambda}, \dot{\boldsymbol{\Lambda}}\right)$ if the input vector $\boldsymbol{U}$ is composed of only $\left(\boldsymbol{\Lambda}, \dot{\boldsymbol{\Lambda}}\right)$. Therefore, both $\boldsymbol{f}$ and $\boldsymbol{\lambda}$ must be bounded as long as $\left(\boldsymbol{\Lambda}, \dot{\boldsymbol{\Lambda}}\right)$ is bounded.

3. Control Input

In this section, a control signal for stable grasping of an object is designed. In the control signal, no knowledge of the grasped object, such as shape, position, or attitude of the grasped object, is necessary. The control signal $\boldsymbol{u}$ is composed of two parts, $\boldsymbol{u}_s$ and $\boldsymbol{u}_{st}$, as follows:

$$\boldsymbol{u} = \boldsymbol{u}_s + \boldsymbol{u}_{st}. \tag{29}$$

The control signal $\boldsymbol{u}_s$ generates a grasping force that is normal to each contact surface.

First, part of the control signal $\boldsymbol{u}_s$ is designed such that the centers of the fingertips approach each other as shown in Fig. 3. This is given as follows:

$$\boldsymbol{u}_s = \frac{f_d}{\sum_{i=1}^{N} r_i}\sum_{j=1}^{N} \boldsymbol{J}_j^{\mathrm{T}}(\boldsymbol{x}_c - \boldsymbol{x}_j) - \boldsymbol{C}\dot{\boldsymbol{q}} + \boldsymbol{g}, \tag{30}$$

where

$$\boldsymbol{x}_c = \frac{1}{N}\sum_{i=1}^{N} \boldsymbol{x}_i, \tag{31}$$

and Eq. (30), $\boldsymbol{C} \in \mathbb{R}^{(N_a+\sum_{i=1}^{N} N_i)\times(N_a+\sum_{i=1}^{N} N_i)} > 0$ is a positive-definite diagonal matrix, which denotes the damping gain of each joint. In addition, $\boldsymbol{g}$ is a gravity compensation term, and f_d is the nominal desired grasping force.

In addition to $\boldsymbol{u}_s$, we introduce another control signal $\boldsymbol{u}_{st}$, which can generate a tangential force to satisfy the dynamic force/torque equilibrium condition in the final state. The new control signal $\boldsymbol{u}_{st}$ is necessary for grasping an arbitrary polyhedral object because when the control input

https://doi.org/10.1017/S0263574712000525 Published online by Cambridge University Press

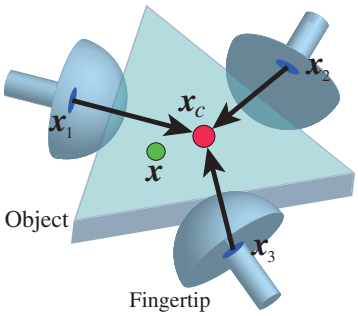

Fig. 3. (Colour online) The centers of the fingertips approach each other.

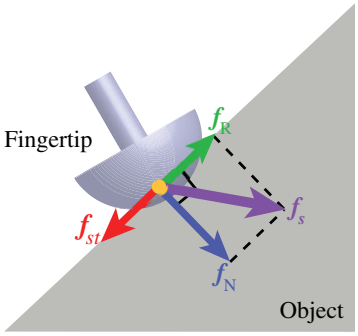

Fig. 4. (Colour online) Contact forces in final state.

$\boldsymbol{u}_s$ is applied to the system, a contact force $\boldsymbol{f}_s$ occurs at each fingertip. The contact force can be decomposed into two orthogonal components, i.e., a normal force component, $\boldsymbol{f}_N$, and a tangential force component, $\boldsymbol{f}_R$, on the object surface, as shown in Fig. 4. The tangential force $\boldsymbol{f}_R$ induces a rolling motion of each fingertip on the object surface. Therefore, in order to satisfy the force/torque equilibrium condition in the final state, the tangential force component of each fingertip $\boldsymbol{f}_R$ must be eliminated because the rolling motion of each fingertip must be prevented. This indicates that the equilibrium condition must be satisfied by only the normal force component of each fingertip $\boldsymbol{f}_N$ if only the control input $\boldsymbol{u}_s$ is applied to the system. However, it is difficult to satisfy this requirement, because how this requirement can be satisfied depends strongly on the mechanical configuration of the hand-arm system as well as the shape of the grasped object. In order to relax this requirement, Arimoto *et al.* and Tahara *et al.*[7–9,14,15] added another control signal to prevent the rolling motion of each fingertip. This additional control term is composed of a time integration of each joint angular velocity, and generates an tangential force opposing $\boldsymbol{f}_R$ to prevent the rolling motion of each fingertip. This additional control term is effective for grasping an object, even if the object is an arbitrary polyhedron. However, the addition of this term induces at least two problems from the stability point of view. The first problem is that the final pose of the overall system cannot be determined specifically in advance because this integration term depends on the total movement of each joint angle. The second problem is that the integration term becomes a disturbance when the grasped object is manipulated, because the integration of each joint angular velocity will interfere with any other controller, not only the control term for stable grasping but also additional position and attitude controllers. The first problem is not so serious with regard to stable grasping because the final pose of the overall system is not important as long as stable grasping is achieved. However, the second problem is quite serious from the viewpoint of dexterity of the hand-arm system.

In the present paper, we introduce another control signal instead of the time integration of each joint angular velocity. The newly proposed additional control signal assigns each fingertip an artificial relative attitude constraint between each fingertip. This constraint acts in the same manner as the time integration of each joint angular velocity, i.e., this constraint generates a tangential force opposing $\boldsymbol{f}_R$. However, this constraint does not interfere any other controller if the multi-fingered hand part has a sufficient number of DOFs because the artificial constraint restricts only the relative attitude of each fingertip by a P-control. As a consequence, a constraint force generated by the artificial constraint works purely to cancel the tangential force, which induces a rolling motion of each fingertip. The introduction of $\boldsymbol{u}_{st}$ is the significant difference compared with the previous studies done by Arimoto *et al.* and Tahara *et al.*[7–9,14,15] The control signal for the relative attitude constraint between each fingertip $\boldsymbol{u}_{st}$ is given as follows:

$$\begin{aligned}\boldsymbol{u}_{st} = K_{st}\sum_{i=1}^{N}\boldsymbol{J}_{\Omega i}^{\mathrm{T}}\{&\boldsymbol{r}_{xfi}\times\left(\boldsymbol{r}_{xfi,(i-1)d}+\boldsymbol{r}_{xfi,(i+1)d}\right)\\&+\boldsymbol{r}_{yfi}\times\left(\boldsymbol{r}_{yfi,(i-1)d}+\boldsymbol{r}_{yfi,(i+1)d}\right)\\&+\boldsymbol{r}_{zfi}\times\left(\boldsymbol{r}_{zfi,(i-1)d}+\boldsymbol{r}_{zfi,(i+1)d}\right)\},\end{aligned}\tag{32}$$

where

$$\boldsymbol{R}_{fi} = \left(\boldsymbol{r}_{xfi},\boldsymbol{r}_{yfi},\boldsymbol{r}_{zfi}\right),\tag{33}$$

$$\begin{aligned}\boldsymbol{R}_{fi,jd} &= \left(\boldsymbol{r}_{xfi,jd},\boldsymbol{r}_{yfi,jd},\boldsymbol{r}_{zfi,jd}\right)\\&= \boldsymbol{R}_{fj}\boldsymbol{R}_{fi,j\mathrm{rel}},\quad (j=(i-1),(i+1)),\end{aligned}\tag{34}$$

and $K_{st} > 0$ is a positive scalar constant. It should be noted that the strength of the artificial constraints can be regulated by the value of K_{st}. In other words, the range of the rolling motion of each fingertip can be roughly adjusted by choosing K_{st} adequately. Rotational matrices $\boldsymbol{R}_{fi}$ and $\boldsymbol{R}_{fi,jd}$ indicate the present attitude and the desired attitude of the ith fingertip respectively. In Eq. (34), $\boldsymbol{R}_{fi,j\mathrm{rel}}$ is a rotational matrix that expresses the relative attitude between the ith and jth fingers as shown in Fig. 5. In the next section, we describe why $\boldsymbol{u}_{st}$ can only generate a tangential force opposing $\boldsymbol{u}_R$ on the object surfaces.

4. Closed-Loop Dynamics

The closed-loop dynamics of the overall system is given by substituting Eq. (29) into the dynamics equations given by Eqs. (19)–(21), such that

https://doi.org/10.1017/S0263574712000525 Published online by Cambridge University Press

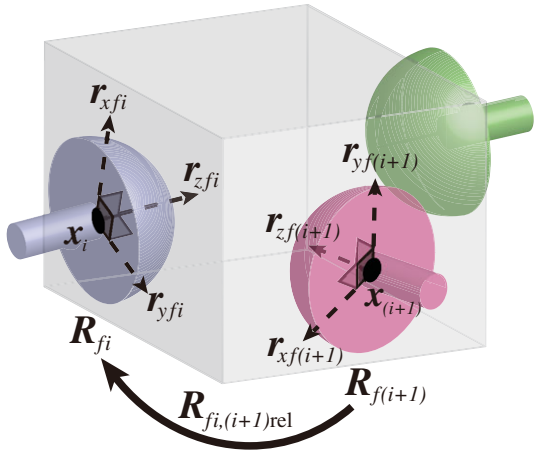

Fig. 5. (Colour online) Relative attitude between ith finger and $i+1$th finger.

for the multi-fingered hand-arm system:

$$\boldsymbol{H}\ddot{\boldsymbol{q}} + \left\{\frac{1}{2}\dot{\boldsymbol{H}} + \boldsymbol{S}\boldsymbol{q} + \boldsymbol{C}\right\}\dot{\boldsymbol{q}} + \sum_{i=1}^{N}\frac{\partial T_i}{\partial \dot{\boldsymbol{q}}}^{\mathrm{T}} + \sum_{i=1}^{N}\boldsymbol{J}_i^{\mathrm{T}}\boldsymbol{R}\cdot\boldsymbol{R}_{Ci}\Delta\boldsymbol{\lambda}_{i1} + \sum_{i=1}^{N}\boldsymbol{J}_{\Omega i}^{\mathrm{T}}\boldsymbol{R}\cdot\boldsymbol{R}_{Ci}\Delta\boldsymbol{\lambda}_{i2} = \boldsymbol{0}, \tag{35}$$

for the object:

$$\boldsymbol{M}\ddot{\boldsymbol{x}} - \sum_{i=1}^{N}\boldsymbol{R}\cdot\boldsymbol{R}_{Ci}\Delta\boldsymbol{\lambda}_{i1} = \boldsymbol{0}, \tag{36}$$

$$\boldsymbol{I}\dot{\boldsymbol{\omega}} + \left\{\frac{1}{2}\dot{\boldsymbol{I}} + \boldsymbol{S}_{\omega}\right\}\boldsymbol{\omega} + \sum_{i=1}^{N}\frac{\partial T_i}{\partial \boldsymbol{\omega}}^{\mathrm{T}} - \sum_{i=1}^{N}(\boldsymbol{x}_i - \boldsymbol{x}) \times \boldsymbol{R}\cdot\boldsymbol{R}_{Ci}\Delta\boldsymbol{\lambda}_{i1} - \sum_{i=1}^{N}(\boldsymbol{R}\cdot\boldsymbol{R}_{Ci}\Delta\boldsymbol{\lambda}_{i2} + K_{st}\boldsymbol{B}_{sti}) = \boldsymbol{0}, \tag{37}$$

where

$$\begin{aligned}
A &= \frac{f_d}{\sum_{j=1}^{N} r_j}\\
\boldsymbol{B}_{sti} &= (\boldsymbol{r}_{xfi}\times\boldsymbol{r}_{xfid}) + (\boldsymbol{r}_{yfi}\times\boldsymbol{r}_{yfid}) + (\boldsymbol{r}_{zfi}\times\boldsymbol{r}_{zfid})\\
\Delta\boldsymbol{\lambda}_{i1} &= (\Delta\lambda_{iX1}, \Delta f_{i1}, \Delta\lambda_{iZ1})^{\mathrm{T}}\\
\Delta\boldsymbol{\lambda}_{i2} &= (\Delta\lambda_{iX2}, \Delta\lambda_{iY2}, \Delta\lambda_{iZ2})^{\mathrm{T}}\\
\Delta\lambda_{iX1} &= -\lambda_{iX} - A\boldsymbol{C}_{iX}^{\mathrm{T}}(\boldsymbol{x}_c - \boldsymbol{x}_i)\\
\Delta f_{i1} &= f_i - A\boldsymbol{C}_{iY}^{\mathrm{T}}(\boldsymbol{x}_c - \boldsymbol{x}_i)\\
\Delta\lambda_{iZ1} &= -\lambda_{iZ} - A\boldsymbol{C}_{iZ}^{\mathrm{T}}(\boldsymbol{x}_c - \boldsymbol{x}_i)\\
\Delta\lambda_{iX2} &= -(r_i - \Delta r_i)\lambda_{iZ} - K_{st}\boldsymbol{C}_{iX}^{\mathrm{T}}\boldsymbol{B}_{sti}\\
\Delta\lambda_{iY2} &= -K_{st}\boldsymbol{C}_{iY}^{\mathrm{T}}\boldsymbol{B}_{sti}\\
\Delta\lambda_{iZ2} &= (r_i - \Delta r_i)\lambda_{iX} - K_{st}\boldsymbol{C}_{iZ}^{\mathrm{T}}\boldsymbol{B}_{sti}
\end{aligned} \tag{38}$$

Taking the sum of the inner product of the output vector $\dot{\boldsymbol{\Lambda}}$ and the closed-loop dynamics expressed by Eqs. (35)–(37) yields

$$\frac{d}{dt}E = -\dot{\boldsymbol{q}}^{\mathrm{T}}\boldsymbol{C}\dot{\boldsymbol{q}} - \sum_{i=1}^{N}\left(T_i + \xi\Delta\dot{r}_i^2\right) \le 0, \tag{39}$$

$$E = K + V + \Delta P, \tag{40}$$

$$K = \frac{1}{2}\dot{\boldsymbol{q}}^{\mathrm{T}}\boldsymbol{H}\dot{\boldsymbol{q}} + \frac{1}{2}\dot{\boldsymbol{x}}^{\mathrm{T}}\boldsymbol{M}\dot{\boldsymbol{x}} + \frac{1}{2}\boldsymbol{\omega}^{\mathrm{T}}\boldsymbol{I}\boldsymbol{\omega}, \tag{41}$$

$$V = V_s + V_{st}, \tag{42}$$

$$V_s = \frac{A}{4N}\left\{\sum_{i=1}^{N}\sum_{j=1}^{N}(\boldsymbol{x}_i - \boldsymbol{x}_j)^2\right\}, \tag{43}$$

$$V_{st} = -K_{st}\sum_{i=1}^{N}\mathrm{tr}\left(\boldsymbol{R}_{fi}^{\mathrm{T}}\boldsymbol{R}_{f(i+1)}\boldsymbol{R}_{fi,(i+1)\mathrm{rel}}\right) \tag{44}$$

$$= K_{st}\sum_{i=1}^{N}(-1 - 2\cos\alpha_i), \tag{45}$$

$$\Delta P = \sum_{i=1}^{N}\int_0^{\delta r_i}\left\{\bar{f}_i(\Delta r_{di} + \phi) - \bar{f}_i(\Delta r_{di})\right\}d\phi, \tag{46}$$

where

$$\delta r_i = \Delta r_i - \Delta r_{di}. \tag{47}$$

In Eq. (47), Δr_{di} is Δr_i when f_i is equal to f_d. In Eq. (45), α_i is the rotational angle of $\boldsymbol{R}_{fi}^{\mathrm{T}}\boldsymbol{R}_{f(i+1)}\boldsymbol{R}_{fi,(i+1)\mathrm{rel}}$. Here, V acts as the artificial potential energy originating from the control input, and K and ΔP are positive as long as $0 \le \Delta r_{di} - \delta r_i < r_i$. In addition,

$$E \ge 0 \tag{48}$$

is satisfied for the case in which K_{st} is designed to satisfy the following equation:

$$K_{st} \le \frac{f_d\sum_{i=1}^{N}\sum_{j=1}^{N}(\boldsymbol{x}_i - \boldsymbol{x}_j)^2}{4N\sum_{k=1}^{N}r_k\sum_{l=1}^{N}(1 + 2\cos\alpha_i)}. \tag{49}$$

Equations (39) and (48) yield

$$\int_0^{\infty}\left\{\dot{\boldsymbol{q}}^{\mathrm{T}}\boldsymbol{C}\dot{\boldsymbol{q}} + \sum_{i=1}^{N}\left(T_i + \xi\Delta\dot{r}_i^2\right)\right\}dt \le E(0) - E(\infty) \le E(0). \tag{50}$$

Equation (50) indicates that the joint angular velocity $\dot{\boldsymbol{q}}(t)$ is squared integrable over time $t \in [0, \infty)$. This means that $\dot{\boldsymbol{q}}(t) \in L^2(0, \infty)$. It is also clear that $\dot{\boldsymbol{x}} \in L^2(0, \infty)$ and $\boldsymbol{\omega} \in L^2(0, \infty)$ by considering the nonholonomic rolling constraint, as shown in Eq. (9). Therefore, the output vector of the overall system $\dot{\boldsymbol{\Lambda}}(t)$ is uniformly continuous and then, from Lemma C1 in ref. [8], $\dot{\boldsymbol{\Lambda}} \to \boldsymbol{0}$ can be given as $t \to \infty$. In addition, from Lemma C3 in ref. [8], $\ddot{\boldsymbol{\Lambda}} \to \boldsymbol{0}$ can also be given as $t \to \infty$ because $\dot{\boldsymbol{\Lambda}} \to \boldsymbol{0}$ as $t \to \infty$. Eventually, the

https://doi.org/10.1017/S0263574712000525 Published online by Cambridge University Press

following equation can be obtained from Eq. (35) such that

$$\begin{cases} \boldsymbol{J}_i^{\mathrm{T}} \boldsymbol{R} \cdot \boldsymbol{R}_{Ci} \Delta \boldsymbol{\lambda}_{i1} \to \boldsymbol{0} \\ \boldsymbol{J}_{\Omega i}^{\mathrm{T}} \boldsymbol{R} \cdot \boldsymbol{R}_{Ci} \Delta \boldsymbol{\lambda}_{i2} \to \boldsymbol{0} \end{cases} \quad \text{as } t \to \infty. \tag{51}$$

Therefore, it is confirmed from Eqs. (35) and (51) that all external forces applied to the hand-arm system converge to zero. The external forces applied to the grasped object are also confirmed to converge to zero by considering Eqs. (36) and (37).

The Jacobian matrix $\boldsymbol{J}_i$ characterizes the relationship between the translational velocity of the center of each fingertip $\dot{\boldsymbol{x}}_i$ and the joint angular velocity vector $\dot{\boldsymbol{q}}$. The other Jacobian matrix $\boldsymbol{J}_{\Omega i}$ also characterizes the relationship between the attitude angular velocity of the center of each fingertip $\boldsymbol{\omega}_i$ and the joint angular velocity vector $\dot{\boldsymbol{q}}$. All column vectors of both Jacobian matrices $\boldsymbol{J}_i^{\mathrm{T}} \boldsymbol{R} \cdot \boldsymbol{R}_{Ci}$ and $\boldsymbol{J}_{\Omega i}^{\mathrm{T}} \boldsymbol{R} \cdot \boldsymbol{R}_{Ci}$ must be mutually independent as long as these Jacobian matrices do not degenerate during movement. The following equations are then obtained from Eq. (51) such that

$$\begin{cases} \Delta \boldsymbol{\lambda}_{i1} \to \boldsymbol{0} \\ \Delta \boldsymbol{\lambda}_{i2} \to \boldsymbol{0} \end{cases} \quad \text{as } t \to \infty. \tag{52}$$

The following equations are obtained from Eqs. (38) and (52):

$$\lambda_{iX} = -A \boldsymbol{C}_{iX}^{\mathrm{T}} (\boldsymbol{x}_c - \boldsymbol{x}_i) = \frac{K_{st}}{r_i - \Delta r_i} \boldsymbol{C}_{iZ}^{\mathrm{T}} \boldsymbol{B}_{sti}, \tag{53}$$

$$\lambda_{iZ} = -A \boldsymbol{C}_{iZ}^{\mathrm{T}} (\boldsymbol{x}_c - \boldsymbol{x}_i) = -\frac{K_{st}}{r_i - \Delta r_i} \boldsymbol{C}_{iX}^{\mathrm{T}} \boldsymbol{B}_{sti}. \tag{54}$$

These equations indicate that the control signal $\boldsymbol{u}_{st}$ generates a counter force to compensate the tangential force generated by the control signal $\boldsymbol{u}_s$, which induces a rolling motion in each fingertip. Moreover, the following equation is obtained from Eqs. (38) and (52):

$$\boldsymbol{C}_{iY}^{\mathrm{T}} \boldsymbol{B}_{sti} \to 0. \tag{55}$$

This equation shows that the grasping forces normal to the object surfaces generated by $\boldsymbol{u}_{st}$ converge to zero. Specifically, $\boldsymbol{u}_{st}$ acts purely to prevent the rolling motion of each fingertip, so that the overall state remains an equilibrium manifold and there is no other effect. On the other hand, based on Eqs. (38) and (52), we can conclude that the grasping force f_i satisfies the following equation:

$$f_i \to \tilde{f}_{id} \quad \text{as } t \to \infty, \tag{56}$$

where

$$\tilde{f}_{id} = \frac{f_d}{\sum_{j=1}^{N} r_j} \boldsymbol{C}_{iY}^{\mathrm{T}} (\boldsymbol{x}_c - \boldsymbol{x}_i). \tag{57}$$

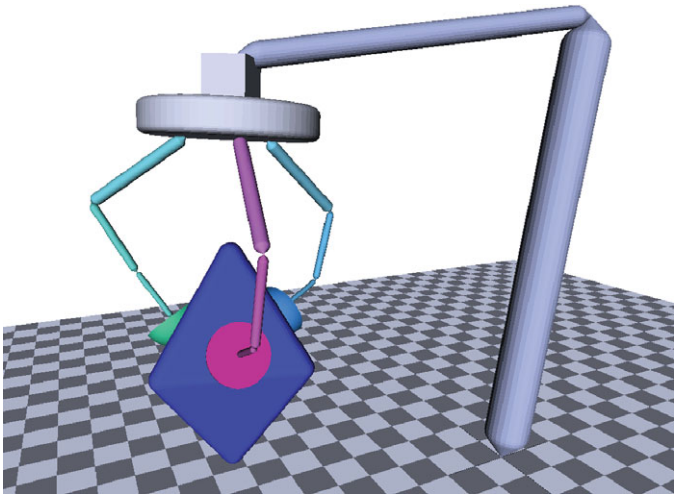

Fig. 6. (Colour online) Simulation for stable grasping.

The equilibrium manifold of the overall system is expressed as follows:

$$\begin{cases} f_i = \tilde{f}_{id}, \quad \boldsymbol{C}_{iY}^{\mathrm{T}} \boldsymbol{B}_{sti} = 0, \quad \dot{\boldsymbol{q}} = \boldsymbol{0}, \\ \dot{\boldsymbol{x}} = \boldsymbol{0}, \quad \boldsymbol{\omega} = \boldsymbol{0} \quad \text{as} \quad t \to \infty. \end{cases} \tag{58}$$

This equation shows that the movement of the overall system converges to zero.

5. Numerical Simulation

A numerical simulation for the grasping of a polyhedral object is conducted here. In this simulation, a desired relative attitude $\boldsymbol{R}_{fi,j\mathrm{rel}}$ in Eq. (34) is configured in order to maintain the initial relative state of all fingertips. It is given as follows:

$$\boldsymbol{R}_{fi,j\mathrm{rel}} = \boldsymbol{R}_{fj\mathrm{ini}}^{\mathrm{T}} \boldsymbol{R}_{fi\mathrm{ini}}, \tag{59}$$

where $\boldsymbol{R}_{fi\mathrm{ini}}$ is a rotational matrix that indicates the initial attitude of the ith fingertip. The hand-arm system used in this simulation incorporates a 5-DOF arm and a three-fingered hand. The hand consists of one 5-DOF finger and two 4-DOF fingers. The grasped object is a hexahedron. Figure 6 shows an example of this simulation. The parameters of the three-fingered hand-arm system and the grasped object are shown in Table I. Table II shows the desired nominal grasping force and the associated gains. Table III shows the initial condition.

Figure 7 shows the transient responses of $\dot{\boldsymbol{q}}$, $\dot{\boldsymbol{x}}$, and $\boldsymbol{\omega}$ indicating that the velocities of the overall system converge to zero. Figure 8 shows the transient responses of $\Delta \boldsymbol{\lambda}_{i1}$ and $\Delta \boldsymbol{\lambda}_{i2}$, which shows that both $\Delta \boldsymbol{\lambda}_{i1}$ and $\Delta \boldsymbol{\lambda}_{i2}$ converge to zero. This means that the total external force nominally applied to the overall system converges to zero. Specifically, the overall state variables are confirmed to converge to the equilibrium manifold, as shown in Eq. (58),

https://doi.org/10.1017/S0263574712000525 Published online by Cambridge University Press

Table I. Physical parameters.

Three-fingered hand-arm system				
1st link length	l_{a1}	1.300 (m)	l_{i1}	0.300 (m)
2nd link length	l_{a2}	1.000 (m)	l_{i2}	0.200 (m)
3rd link length	l_{a3}	0.175 (m)	l_{i3}	0.140 (m)
1st mass center	l_{ga1}	0.650 (m)	l_{gi1}	0.150 (m)
2nd mass center	l_{ga2}	0.500 (m)	l_{gi2}	0.100 (m)
3rd mass center	l_{ga3}	0.0875 (m)	l_{gi3}	0.070 (m)
1st mass	m_{a1}	1.300 (kg)	m_{i1}	0.250 (kg)
2nd mass	m_{a2}	1.000 (kg)	m_{i2}	0.150 (kg)
3rd mass	m_{a3}	0.400 (kg)	m_{i3}	0.100 (kg)
1st Inertia $\boldsymbol{I}_{a1}$	diag (7.453, 7.453, 0.260) $\times 10^{-1}$(kg · m^2)			
2nd Inertia $\boldsymbol{I}_{a2}$	diag (3.397, 3.397, 0.128) $\times 10^{-1}$(kg · m^2)			
3rd Inertia $\boldsymbol{I}_{a3}$	diag (0.291, 0.291, 0.500) $\times 10^{-1}$(kg · m^2)			
1st Inertia $\boldsymbol{I}_{i1}$	diag (7.725, 7.725, 0.450) $\times 10^{-3}$(kg · m^2)			
2nd Inertia $\boldsymbol{I}_{i2}$	diag (2.060, 2.060, 0.120) $\times 10^{-3}$(kg · m^2)			
3rd Inertia $\boldsymbol{I}_{i3}$	diag (0.538, 0.538, 0.031) $\times 10^{-3}$(kg · m^2)			
Radius of fingertip r_i	0.070 (m)			
k_i	1.000×10^5(N/m^2)			
ξ_i	$1.000\times \left(2r_i\Delta r_i - \Delta r_i^2\right)\pi$(Ns/m)			
b_i	$1.000\times \left(2r_i\Delta r_i - \Delta r_i^2\right)\pi \times 10^4$(Ns/m^2)			

Object	
Mass m	0.0018 (kg)
Length of each side	0.42(m)
Inertia $\boldsymbol{I}$	diag (1.354, 0.765, 1.354) $\times 10^{-3}$(kg · m^2)

Table II. Desired grasping force and gains.

f_d	10.0
K_{st}	5.238×10^{-2}
$\boldsymbol{C}_a$	diag (1.003, 0.651, 0.735, 0.278, 0.177) $\times 10^{-1}$ (Ns·m/rad)
$\boldsymbol{C}_1$	diag (0.606, 0.687, 0.786, 0.642, 0.198) $\times 10^{-2}$ (Ns·m/rad)
$\boldsymbol{C}_2$	diag (0.468, 0.780, 0.318, 0.099) $\times 10^{-2}$ (Ns·m/rad)
$\boldsymbol{C}_3$	diag (0.648, 0.780, 0.318, 0.099) $\times 10^{-2}$ (Ns·m/rad)

Table III. Initial condition.

$\dot{\boldsymbol{q}}$	$\boldsymbol{0}$ (rad/s)
$\boldsymbol{q}_a$	$(-0.176, -1.701, 1.904, 1.360, 0.520)^{\mathrm{T}}$ (rad)
$\boldsymbol{q}_{01}$	$(0.000, 0.035, -0.995, 1.588, 0.122)^{\mathrm{T}}$ (rad)
$\boldsymbol{q}_{02}$	$(0.011, -0.922, 1.219, 0.836)^{\mathrm{T}}$ (rad)
$\boldsymbol{q}_{03}$	$(-0.052, -0.803, 1.065, 0.890)^{\mathrm{T}}$ (rad)
$\dot{\boldsymbol{x}}$	$\boldsymbol{0}$ (m/s)
$\boldsymbol{x}$	$(-0.126, 0.423, 0.776)^{\mathrm{T}}$ (m)
$\boldsymbol{\omega}$	$\boldsymbol{0}$ (rad/s)
$\boldsymbol{R}$	$\begin{bmatrix} 0.74 & 0.07 & -0.67 \\ -0.04 & 1.00 & 0.05 \\ 0.68 & -0.01 & 0.74 \end{bmatrix}$

and thereby the dynamic force/torque equilibrium condition for the immobilization of the object is satisfied at the final state.

6. Experiments

In the present study, experiments to examine the grasping of a polyhedral object were conducted using a prototype setup. In the experiments, only the three-fingered robotic hand, as shown in the left-hand side of Fig. 9, is used in the experiments. Note that the proposed controller is applicable not only to the hand-arm system but also to the hand system. The prototype robotic hand consists of three 4-DOF fingers. The structure of each finger is shown in the right-hand side of Fig. 9. Each parameter of the hand system is shown in Table IV. In addition, Table V shows the specifications of the actuator used in the system. Each joint angle is obtained by an encoder, and the sampling period of the servo-loop is 1 ms. Figure 10 shows the system configuration. In the experiments, two types of grasped objects were used: a triangular prism and a cube. The parameters of these objects are listed in Table VI. In the experiments, we selected styrene foam as the material of the grasped object and ignore the effect of gravity. Table VII shows the desired nominal grasping force and gains.

A photograph of the experiment to examine stable grasping of a triangular prism is shown in Fig. 11. Figure 12 shows the transient responses of $\dot{\boldsymbol{q}}$ in the experiments for stable

https://doi.org/10.1017/S0263574712000525 Published online by Cambridge University Press

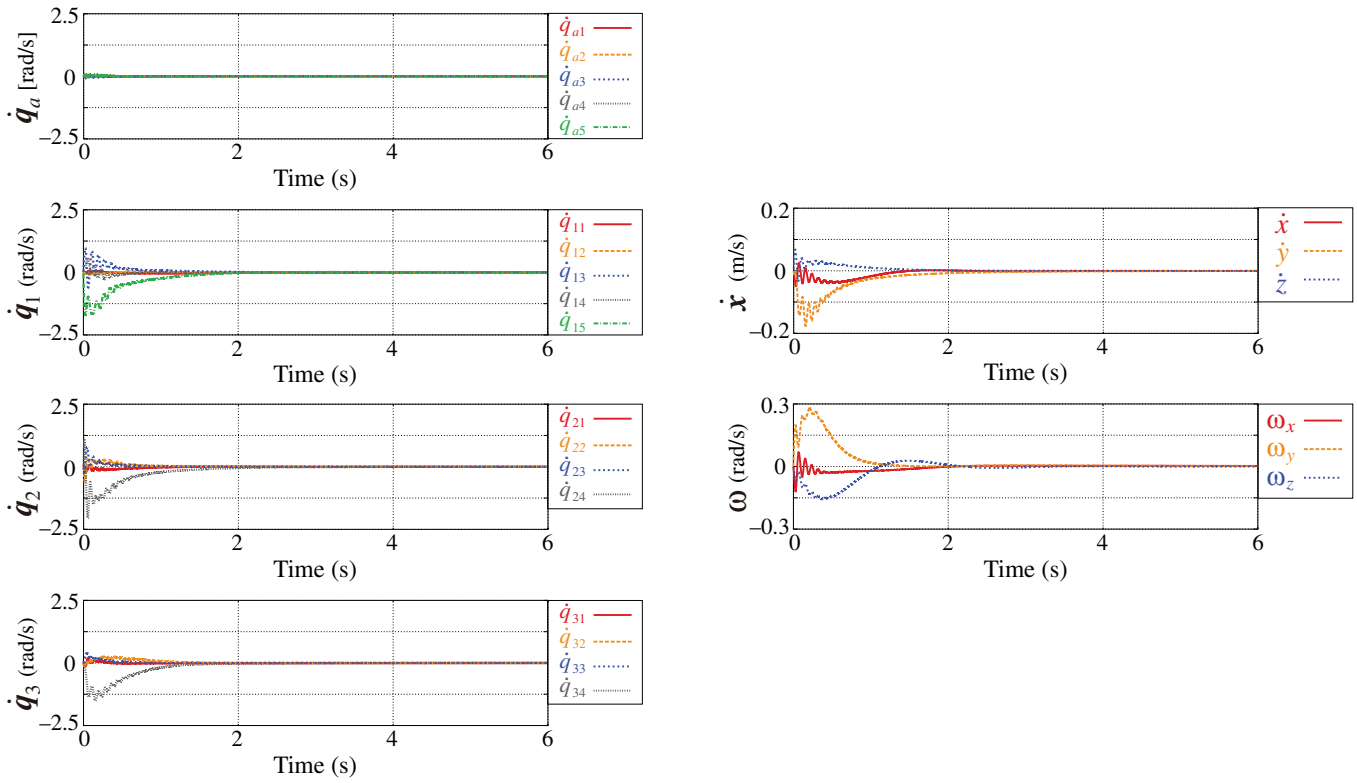

Fig. 7. (Colour online) Transient responses of angular velocity of the hand-arm system $\dot{\boldsymbol{q}}$ and the translational and rotational velocities of the grasped object $\dot{\boldsymbol{x}}$ and $\boldsymbol{\omega}$.

grasping of both the triangular prism and the cube. This figure shows that the velocities of the overall system converge to zero, that is, the proposed method can accomplish stable object grasping. In particular, the force/torque equilibrium condition cannot be satisfied when the grasping force normal to the object surface is only considered in the case of grasping the cuboid as in Fig. 13. In contrast, the equilibrium condition can be satisfied when not only the normal grasping forces but also the tangential grasping forces generated by the control signal $\boldsymbol{u}_{st}$ are utilized effectively even in the case of grasping the cuboid. The gravity effect to the grasped object is quite small because of its small mass, and thereby it can be negated

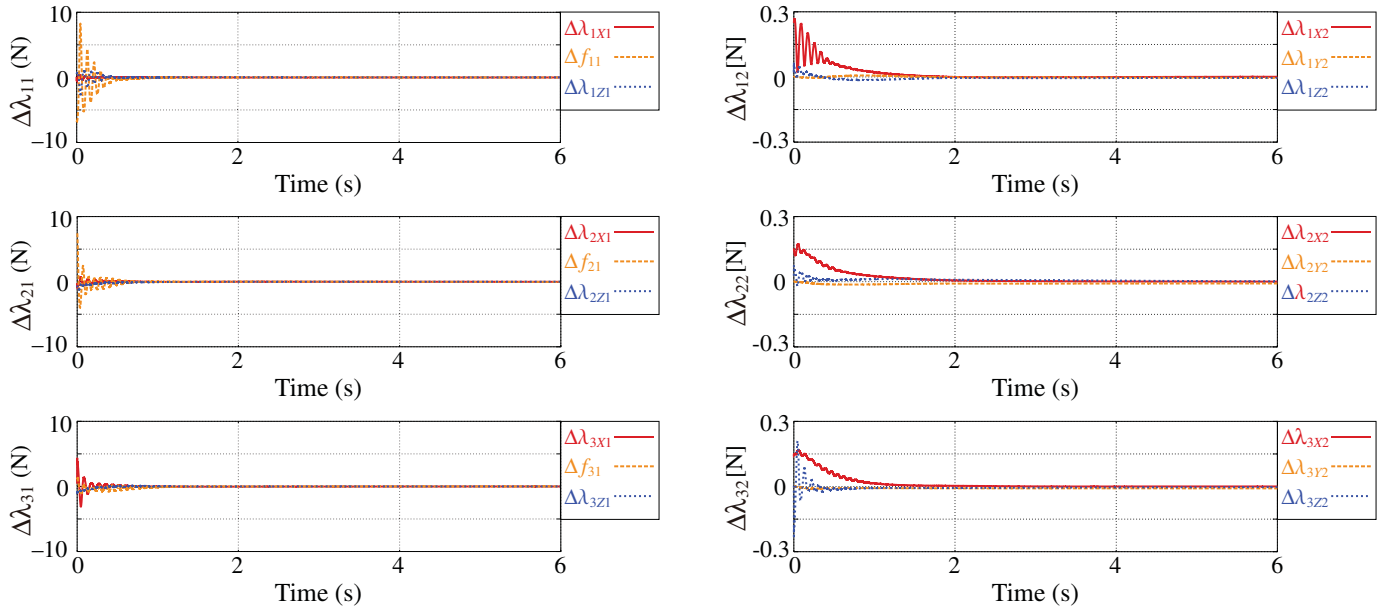

Fig. 8. (Colour online) Transient responses of $\Delta\boldsymbol{\lambda}_{i1}$ and $\Delta\boldsymbol{\lambda}_{i2}$.

https://doi.org/10.1017/S0263574712000525 Published online by Cambridge University Press

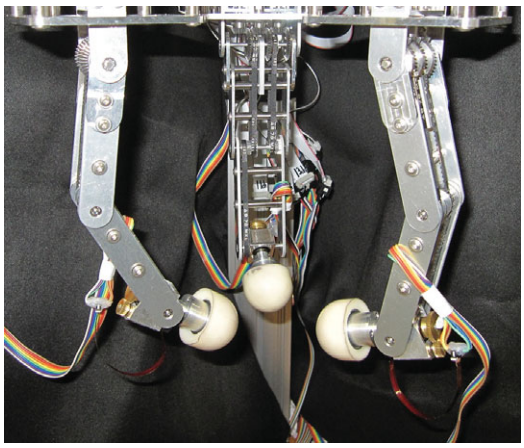

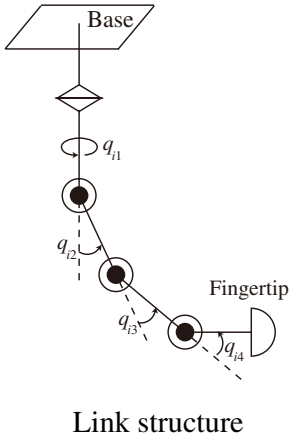

Fig. 9. (Colour online) Three-fingered robotic hand.

Table IV. Physical parameters.

Three-fingered robotic hand	
1st link length l_{i1}	0.064 (m)
2nd link length l_{i2}	0.064 (m)
3rd link length l_{i3}	0.030 (m)
1st mass center l_{gi1}	0.023 (m)
2nd mass center l_{gi2}	0.035 (m)
3rd mass center l_{gi3}	0.010 (m)
1st mass m_{i1}	0.038 (kg)
2nd mass m_{i2}	0.024 (kg)
3rd mass m_{i3}	0.054 (kg)
(Fingertip)	
Radius r_i	0.015 (m)
Physical properties s_i	2.390×10^6 (N/m^2)

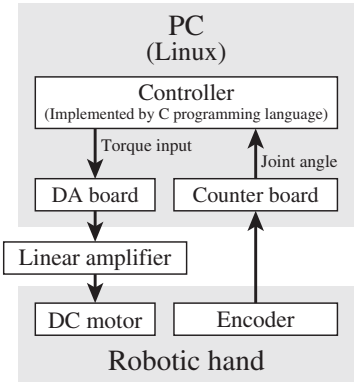

Fig. 10. System configuration.

Table V. Specifications of the actuators.

Motor Type	DC
Maximum speed (rpm)	9550
Maximum torque (Nm)	257
Gear ratio	5.4 : 1
Resolution [deg]	0.0167

due to friction forces on each joint and the tangential forces generated by $\boldsymbol{u}_{st}$.

7. Conclusion

The present paper described a novel stable grasping method for the grasping of an arbitrary polyhedral object. We formulated the nonholonomic rolling constraint between each fingertip and the object surface and presented the overall dynamics, including the effect of the rolling constraint between fingertips and object surfaces. A new control signal was proposed, and the stability of the overall system was demonstrated through analysis of the closed-loop dynamics.

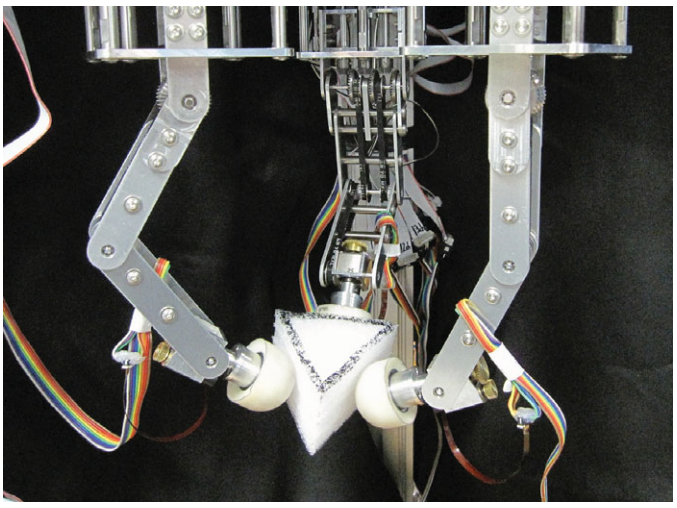

Fig. 11. (Colour online) Stable grasping of the triangular prism.

Then, numerical simulations were conducted in order to demonstrate that the proposed controller enables an arbitrary polyhedral object to be grasped. In addition, we demonstrated the usefulness of the proposed controller in a practical

https://doi.org/10.1017/S0263574712000525 Published online by Cambridge University Press

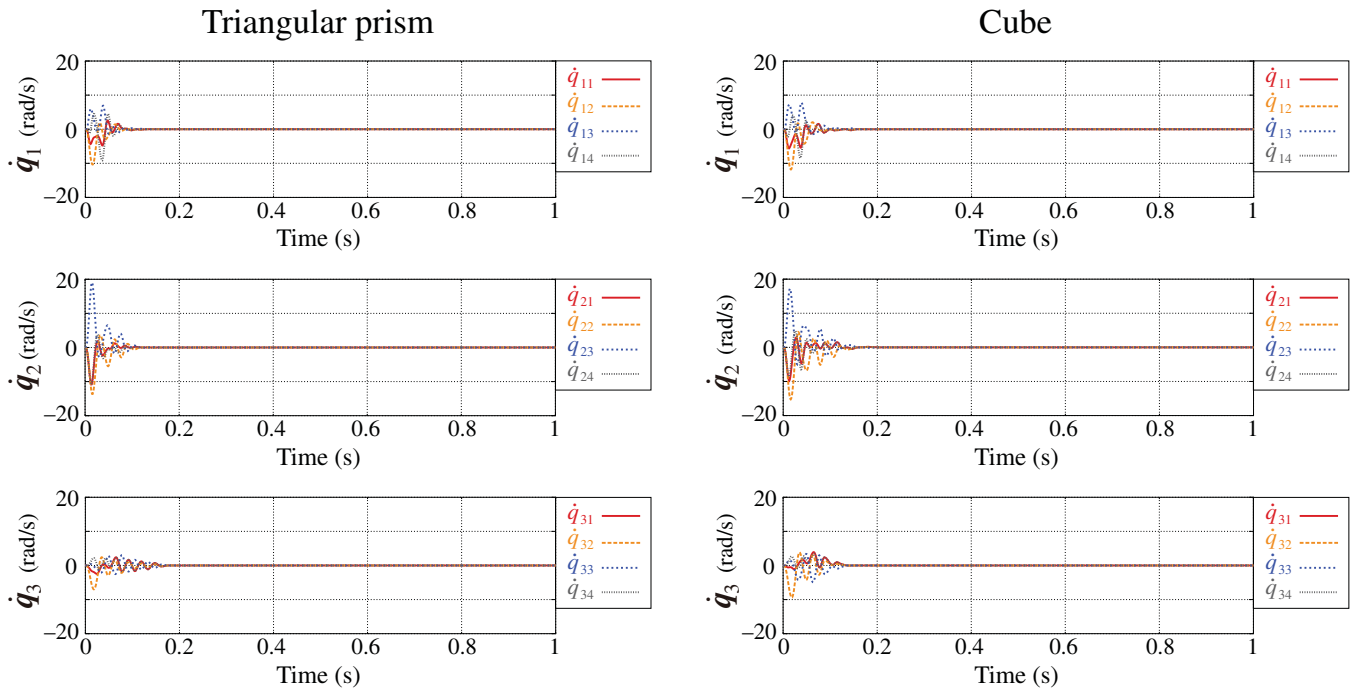

Fig. 12. (Colour online) Transient responses of angular velocity of the hand-arm system $\dot{\boldsymbol{q}}$ during grasping of the triangular prism and the cube.

Table VI. Details of the grasped object.

Triangular pyramid	
Mass m	0.0015 (kg)
Material	Styrene foam
(Figure)	
Length of side of triangle	0.060 (m)
Height	0.039 (m)
Cube	
Mass m	0.0021 (kg)
Material	Styrene foam
(Figure)	
$0.048 \times 0.048 \times 0.048$ (m)	

Table VII. Nominal desired grasping force and gains.

f_d	5.0
K_{st}	5.0×10^{-3}
$\boldsymbol{C}_1$	diag (0.04, 0.04, 0.03, 0.02) $\times 10^{-2}$ (Ns·m/rad)
$\boldsymbol{C}_2$	diag (0.04, 0.04, 0.03, 0.02) $\times 10^{-2}$ (Ns·m/rad)
$\boldsymbol{C}_3$	diag (0.04, 0.04, 0.03, 0.02) $\times 10^{-2}$ (Ns·m/rad)

situation through experiments using a prototype hand system. The effectiveness of the proposed method in case it is combined with the position and attitude controller for the grasped object has been demonstrated through numerical simulations in ref. [17]. The results showed that the position and attitude of the grasped object converges to the desired values. Therefore, we can say that the proposed controller does not disturb and interfere with manipulation task. As a future work, we will verify the performance of this combined controller[17] theoretically and experimentally.

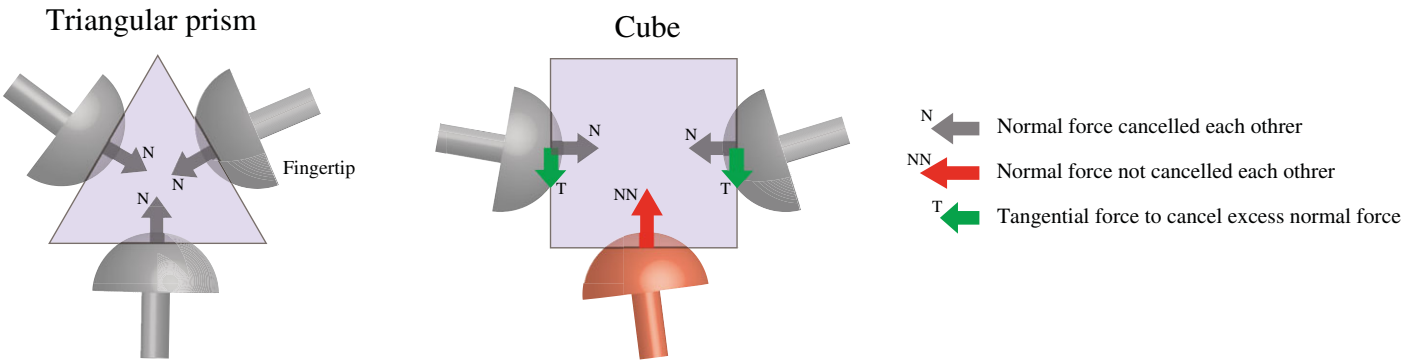

Fig. 13. (Colour online) Contact forces during grasping of a triangular prism and a cube.

https://doi.org/10.1017/S0263574712000525 Published online by Cambridge University Press

Acknowledgment
The present study was supported in part by a Grant-in-Aid for JSPS Fellows.

References

1. M. R. Cutkosky, *Robotic Grasping and Fine Manipulation* (Kluwer Academic, Dordrecht, Netherlands, 1985).
2. R. M. Murray, Z. Li and S. S. Sastry, *Mathematical Introduction to Robotic Manipulation* (CRC Press, Boca Raton, FL, 1994).
3. K. B. Shimoga, "Robot grasp synthesis algorithms: A survey," *Int. J. Robot. Res.* **15**(3), 230–266 (1996).
4. A. M. Okamura, N. Smaby and M. R. Cutkosky, "An Overview of Dexterous Manipulation," **In**: *Proceedings of the IEEE International Conference on Robotics and Automation*, San Francisco, CA (2000) pp. 255–262.
5. A. Bicchi, "Hands for dexterous manipulation and robust grasping: A difficult road towards simplicity," *IEEE Trans. Robot. Automat.* **16**(6), 652–662 (2000).
6. A. Bicchi, "On the closure properties of robotic grasping," *Int. J. Robot. Res.* **14**(4), 319–334 (1995).
7. S. Arimoto, P. T. A. Nguyen, H.-Y. Han and Z. Doulgeri, "Dynamics and control of a set of dual fingers with soft tips," *Robotica* **18**(1), 71–80 (2000).
8. S. Arimoto, "A differential-geometric approach for 2-D and 3-D object grasping and manipulation," *Annu. Rev. Control* **31**(2), 189–209 (2007).
9. S. Arimoto, *Control Theory of Multi-Fingered Hands. A Modelling and Analytical-Mechanics Approach for Dexterity and Intelligence* (Springer, New York, 2008).
10. D. Montana, "The kinematics of contact and grasp," *Int. J. Robot. Res.* **7**(3), 17–32 (1988).
11. A. Cole, J. Hauser and S. Satry, "Kinematics and control of multifingered hands with rolling contacts," *IEEE Trans. Automat. Contr.* **34**(4), 398–404 (1989).
12. L. Han and J. Trincle, "Dexterous manipulation by rolling and finger gaiting," **In**: *Proceedings of the IEEE International Conference on Robotics and Automation*, Leuven, Belgium (1998) pp. 730–735.
13. K. Harada, M. Kaneko and T. Tsuji, "Rolling-based manipulation for multiple objects," **In**: *Proceedings of the IEEE International Conference on Robotics and Automation*, San Francicso, CA (2000) pp. 3887–3894.
14. K. Tahara, S. Arimoto and M. Yoshida, "Dynamic Force/Torque Equilibrium for Stable Grasping by a Triple Robotic Fingers System," **In**: *Proceedings of the IEEE/RSJ International Conferences on Intelligent and Robotic Systems*, St. Louis, MO (2009) pp. 2257–2263.
15. K. Tahara, S. Arimoto and M. Yoshida, "Dynamic Object Manipulation Using a Virtual Frame by a Triple Soft-Fingered Robotic Hand," **In**: *Proceedings of the IEEE International Conference on Robotics and Automation*, Anchorage, AK (2010) 4322–4327.
16. J.-H. Bae, S. Arimoto, R. Ozawa, M. Sekimoto and M. Yoshida, "A Unified Control Scheme for a Whole Robotic Arm-Fingers System in Grasping and Manipulation," **In**: *Proceedings of the IEEE International Conference on Robotics and Automation*, Orlando, FL (2006) pp. 2131–2136.
17. A. Kawamura, K. Tahara, R. Kurazume and T. Hasegawa, "Dynamic Object Manipulation Using a Multi-Fingered Hand-Arm System: Enhancement of a Grasping Capability Using Relative Attitude Constraints of Fingers," **In**: *Proceedings of the International Conference on Advanced Robotics*, St. Paul, MN (2011) pp. 8–14.